

## Implications of the nanoHertz Gravitational-Wave Background for Galactic Feedback and Massive Black Hole Growth

MEGAN TAYLOR TILLMAN,<sup>1</sup> BLAKESLEY BURKHART,<sup>2,1</sup> CHIARA M. F. MINGARELLI,<sup>3,2</sup> J. ANDREW CASEY-CLYDE,<sup>4,3</sup>  
 LARS HERNQUIST,<sup>5</sup> SOWNAK BOSE,<sup>6</sup> ENIKO REGOS,<sup>7</sup> AND CÉSAR HERNÁNDEZ-AGUAYO<sup>8</sup>

<sup>1</sup>Department of Physics and Astronomy, Rutgers University, 136 Frelinghuysen Rd, Piscataway, NJ 08854, USA

<sup>2</sup>Center for Computational Astrophysics, Flatiron Institute, 162 5th Avenue, New York, NY, 10010, USA

<sup>3</sup>Department of Physics, Yale University, New Haven, CT 06520, USA

<sup>4</sup>Department of Physics, University of Connecticut, 196 Auditorium Road, U-3046, Storrs, CT 06269-3046, USA

<sup>5</sup>Center for Astrophysics — Harvard & Smithsonian, 60 Garden St., Cambridge, MA 02138, USA

<sup>6</sup>Institute for Computational Cosmology, Department of Physics, Durham University, South Road, Durham DH1 3LE, UK

<sup>7</sup>HUN-REN CSFK Konkoly Observatory, Budapest, Konkoly Thege M 15-17

<sup>8</sup>LadHyX UMR CNRS 7646, Ecole Polytechnique, Institut Polytechnique de Paris, 91128 Palaiseau Cedex, France

### ABSTRACT

We investigate how pulsar timing array (PTA) measurements of the nanoHertz gravitational-wave background (GWB) can constrain models for the growth history of supermassive black holes (SMBHs) and how active galactic nucleus (AGN) and stellar feedback models can affect GWB predictions. Feedback regulates supermassive black hole (SMBH) growth, altering the black hole mass function (BHMF). Using BHMFs drawn from multiple cosmological simulation suites including IllustrisTNG, MillenniumTNG, Simba, and CAMELS, and combining these with a quasar-based SMBH binary population framework, we predict the resulting GWB amplitude under a range of different stellar and AGN feedback prescriptions. We find that the choice of both stellar and AGN feedback models alters the high-mass end of the BHMF and changes the predicted GWB amplitude by up to a factor of 2 for the fiducial simulations and a factor 10 for extreme feedback variations in CAMELS. Models with inefficient or absent AGN feedback produce abundant SMBHs and yield GWB amplitudes consistent with PTA data, yet fail in producing realistic galaxies. Fiducial models of AGN and stellar feedback suppress SMBH growth too much and under-predict the expected signal, an effect which could possibly be mitigated by more realistic black hole seeding and growth prescriptions. The mismatch between the GWB amplitudes predicted by cosmological simulations and those observed by PTAs suggests that SMBH growth is more efficient or occurs earlier than captured by current models. This demonstrates that PTA measurements provide a powerful new probe of feedback physics and the SMBH population.

**Keywords:** Gravitational wave astronomy (675) — Gravitational waves (678) — Quasars (1319) — Supermassive black holes (1663)

### 1. INTRODUCTION

Supermassive black holes (SMBHs) grow through accretion and mergers, and in doing so release enormous amounts of energy into their surroundings (Schmidt 1963; White & Rees 1978; Kulier et al. 2015). This process, broadly known as active galactic nucleus (AGN) feedback, regulates both the growth of SMBHs and the evolution of their host galaxies. Feedback can occur in radiative or kinetic modes, heating and expelling gas from galactic centers, suppressing further accretion, and altering star formation histories (Di Matteo et al. 2005; Fabian 2012; Heckman & Best 2014; Weinberger et al.

2023). Because AGN feedback controls the fueling of SMBHs, it leaves a direct imprint on the black hole mass function (BHMF) (Ni et al. 2025). Stronger feedback can truncate black hole growth, while weaker feedback allows more massive SMBHs to form, shifting the shape and normalization of the BHMF (Steinborn et al. 2015; Sunseri et al. 2025).

The low frequency gravitational wave background (GWB) recently measured by pulsar timing arrays (PTAs, Agazie et al. 2023; Antoniadis et al. 2023; Readon et al. 2023; Xu et al. 2023; Miles et al. 2024) is likely generated by the incoherent superposition of SMBH binaries across cosmic time. This makes the GWB a sen-

sitive probe of the overall SMBH population in the Universe and the binary merger rate (Kelley 2024). Its amplitude depends sensitively on the mass of the SMBHs, and therefore on the underlying BHMF (Phinney 2001; Sesana et al. 2008). Casey-Clyde et al. (2022) made this connection explicit by building a quasar-based SMBH population model tied to an empirically constrained BHMF. They showed that the GWB amplitude can be decomposed into contributions from the BHMF, the number density of binaries, and the cosmological volume. In this framework, any modification to the BHMF directly propagates into a change in the predicted GWB amplitude.

Since AGN feedback regulates SMBH growth via accretion, it is one of the dominant physical processes shaping the BHMF, in addition to mergers. The work presented here examines how both AGN and stellar feedback models modify the BHMF and, by extension, the GWB amplitude. Many previous studies have extracted SMBH merger rates from large-volume simulations and translated them into PTA-band predictions (Marinacci et al. 2025). For example, using the ILLUSTRISS simulation, Kelley et al. (2017b) showed that the SMBH merger population naturally produces a nanoHertz background at levels within reach of PTAs, and Sykes et al. (2022) employed MASSIVEBLACK-II to forecast the GWB from its SMBH merger catalog. Kozhikkal et al. (2024) explored how the black hole–bulge mass relation and its redshift evolution, calibrated with multiple cosmological simulations, impact predictions for the GWB. The ASTRID simulation follows the orbital decay and pairing of SMBHs self-consistently during the run, providing so-called “on-the-fly” black hole dynamics that reduce the need for subgrid merger prescriptions (Ni et al. 2022). Chen et al. (2025) find that ASTRID yields a GWB amplitude amounting to roughly half of the observed PTA signal, underscoring the sensitivity of the background to assumptions about SMBH mergers. These works complement ours by highlighting how host-galaxy scaling relations influence merger rates and the expected GWB amplitude.

These studies demonstrate that cosmological simulations can predict a GWB of the correct order of magnitude, but they do not explicitly explore how AGN feedback feeds into the GWB amplitude through the BHMF. We conduct such an analysis herein. Using the methodology of Casey-Clyde et al. (2022), we conduct a broad comparison of the BHMF and predicted GWB amplitude of three different cosmological hydrodynamic models: Simba, IllustrisTNG, and MillenniumTNG and also explore extreme feedback parameter variations of these models using the CAMELS simulations. The paper is

laid out as follows. In Section 2 we describe how the broad range of AGN feedback models from IllustrisTNG, MillenniumTNG, Simba, and CAMELS and how these give rise to different BHMFs. In Section 3, we review how Casey-Clyde et al. (2022) links the BHMF to the GWB amplitude, while in Section 4 we report our results. We discuss our results in 5 and summarize our conclusions in Section 6.

## 2. SIMULATIONS OVERVIEW

We explore the IllustrisTNG, MillenniumTNG, Simba, and CAMELS simulation suites and analyze how variations in the galactic feedback models impact the predicted BHMF. Differences in the predicted BHMF have implications for measurements of the stochastic GWB amplitude. For each suite, we also analyze a set of simulations with varying box sizes to conduct a convergence study. This is important because the GWB amplitude is sensitive to the high mass end of the BHMF, which itself is sensitive to box size. In the following subsections, we describe the different cosmological hydrodynamic simulation models analyzed and the variations of said models explored. We also describe how we extract the BHMF from these simulations.

### 2.1. *The IllustrisTNG and MillenniumTNG Simulations*

The IllustrisTNG simulations are run using the AREPO code (Springel 2010; Weinberger et al. 2020) and model gravitational interactions through the TreePM algorithm (Springel et al. 2005). Radiative cooling, including line cooling, free-free emission, and inverse Compton cooling, is modeled as described in Katz et al. (1996). Metal and metal-line cooling are described in Vogelsberger et al. (2012, 2013). IllustrisTNG assumes ionizing equilibrium and a uniform ionizing background model, which accounts for on-the-fly hydrogen self-shielding (Faucher-Giguère et al. 2009; Rahmati et al. 2013). Star formation and the ISM subgrid model are from Springel & Hernquist (2003), and enrichment is modeled from Type Ia and II Supernovae (SNe), asymptotic giant branch (AGB) stars, and neutron star mergers. The IllustrisTNG simulations use the cosmological parameters:  $\Omega_m = 0.3089$ ,  $\Omega_\Lambda = 0.6911$ ,  $\Omega_b = 0.0486$ ,  $H_0 = 67.74$  km/s/Mpc,  $\sigma_8 = 0.8159$ , and  $n_s = 0.9667$ .

IllustrisTNG models galactic feedback from both stars and AGN. Stellar feedback is modeled as kinetic (with a thermal sub-component) galactic winds that are temporarily hydrodynamically decoupled. These winds are stochastically and isotropically ejected from star-forming gas. This model is further described in Pillepich et al. (2018).

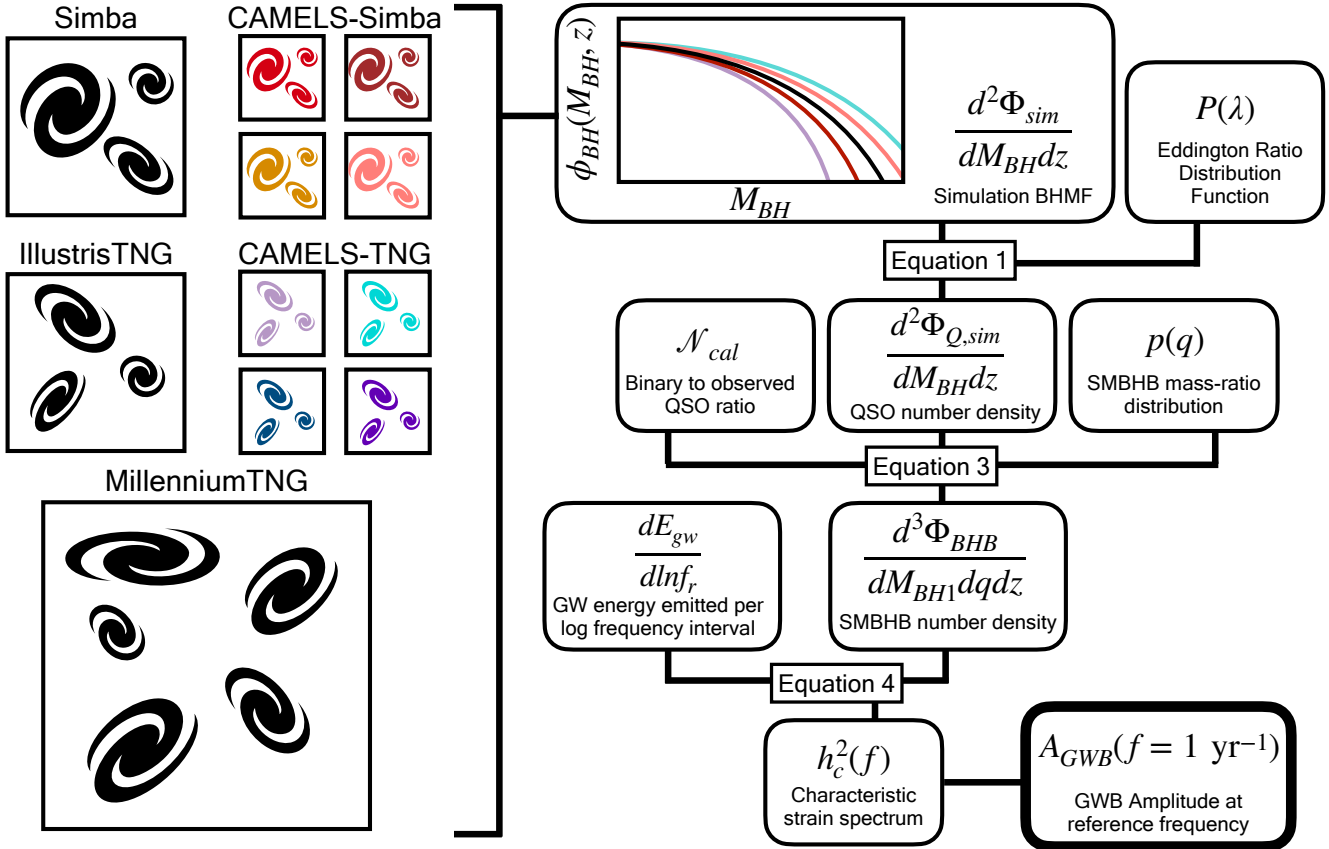


**Figure 1.** Graphic illustrating the pipeline used to obtain the GWB amplitude from the simulation BHMFs. We explore different simulation models (left-side), MillenniumTNG/IllustrisTNG and Simba, and variations of said models using the CAMELS simulation suites. These different simulations predict different BHMFs which are used in our semi-analytic model to calculate the characteristic strain spectrum (right-side), described in Section 3.

In IllustrisTNG, SMBHs are seeded with mass  $M_{\text{BHseed}} = 8 \times 10^5 M_{\odot}/h$  in halos with mass  $M_{\text{FoF}} > 5 \times 10^{10} M_{\odot}/h$ . BH accretion in IllustrisTNG uses the Bondi (1952) prescription, capped at the Eddington limit. AGN feedback includes three modes: thermal, kinetic, and radiative. The radiative mode is always on and adds the radiation flux of the SMBH to the cosmic ionizing background, heating the gas nearest to the host halo. Which of the other two modes is active depends on the accretion rate of the BH. At high accretion rates, the thermal feedback mode is active, while at lower accretion rates, the kinetic feedback mode is active. For both of these modes, energy is injected into the ‘feedback sphere’ of the SMBH. Unlike stellar feedback, AGN feedback in IllustrisTNG is never decoupled hydrodynamically. For more information on the IllustrisTNG model, we refer the reader to Pillepich et al. (2018) and Nelson et al. (2019).

We analyze three different IllustrisTNG simulations, each with different box sizes but all implementing identical physics. The smallest box size has a co-moving

side length of  $35 \text{ Mpc}/h$  with  $2160^3$  gas particles and an initial mass resolution of  $8.5 \times 10^4 M_{\odot}$  (TNG50). The next box has a side length of  $75 \text{ Mpc}/h$  with  $1820^3$  gas particles and an initial mass resolution  $1.4 \times 10^6 M_{\odot}$  (TNG100). The largest box has a side length of  $205 \text{ Mpc}/h$  with  $2500^3$  gas particles and an initial mass resolution  $1.1 \times 10^7 M_{\odot}$  (TNG300). We use these different box sizes to explore convergence of the BHMF.

We also utilize the MillenniumTNG simulation to test the convergence of the BHMF. The MillenniumTNG simulation uses identical physics and parameters to IllustrisTNG, with only a few minor modifications where small issues found during and after the IllustrisTNG run were fixed (Pakmor et al. 2023). The MillenniumTNG simulation has a co-moving box side length of  $500 \text{ Mpc}/h$  with  $4320^3$  gas particles and an initial mass resolution of  $3.1 \times 10^7 M_{\odot}$  (MTNG740). We discuss the impact of box size on predictions for the GWB amplitude in Section 5.

## 2.2. The Simba Simulations

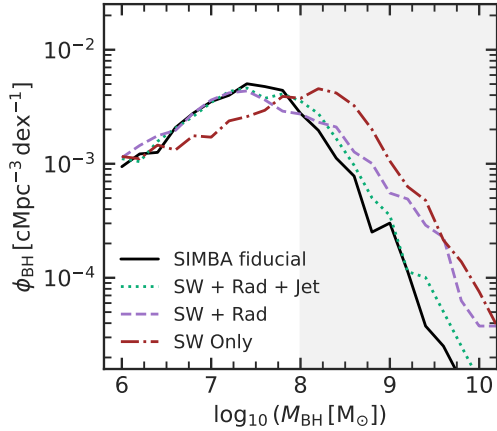


**Figure 2.** The  $z = 0$  BHMF predicted by the Simba simulation model when implementing different AGN feedback modes. The volume, resolution, cosmology, and all other astrophysics are the same in these simulations. This illustrates how much variation can occur in the predicted BHMF due to AGN feedback. Variations on the high mass end ( $M_{\text{BH}} \gtrsim 10^8 M_\odot$ , marked by the shaded grey region) of the mass function will most impact the gravitational wave background amplitude with higher mass SMBHs contributing more.

The Simba simulations are run with GIZMO’s meshless finite mass hydrodynamics (Hopkins 2015) and employ state-of-the-art subgrid physical processes to form realistic galaxies (Davé et al. 2019). Based on GADGET-3 (Springel et al. 2005), the GIZMO gravity solver evolves dark matter and gas simultaneously with gravitational and pressure forces. It models shocks via a Riemann solver with no artificial viscosity. Radiative cooling and photoionizing heating are modeled with Grackle3.0 which includes non-equilibrium evolution of primordial elements, a partially-uniform ionizing background, hydrogen self-shielding, and metal cooling (Smith et al. 2017; Haardt & Madau 2012; Rahmati et al. 2013). The Simba simulations utilize cosmological parameters:  $\Omega_m = 0.3$ ,  $\Omega_\Lambda = 0.7$ ,  $\Omega_b = 0.048$ ,  $H_0 = 68$  km/s/Mpc,  $\sigma_8 = 0.82$ , and  $n_s = 0.97$ .

The Simba simulations model both stellar and AGN feedback. Simba tracks chemical enrichment from Type Ia SNe, Type II SNe and from AGB stars (Li et al. 2019). Stellar feedback is modeled through kinetic galactic winds that are temporarily hydrodynamically-decoupled, two-phase, and metal-enriched. The SNe feedback prescriptions are based on the FIRE zoom-in simulations (Hopkins et al. 2014; Muratov et al. 2015; Anglés-Alcázar et al. 2017b).

In Simba, SMBHs are seeded with mass  $M_{\text{BHseed}} = 10^4 M_\odot/h$  in galaxies that do not already contain a SMBH based on a stellar mass threshold  $M_* \gtrsim 10^{9.5} M_\odot$ .

BH accretion is based on both the gravitational torque and Bondi accretion models, with cold and hot gas accreting in different modes (Bondi 1952; Hopkins & Quataert 2011; Anglés-Alcázar et al. 2017a). Similarly, AGN feedback is modeled in two modes: with high accretion rate mass loading outflows (the radiative mode) and low accretion rate jets (the jet mode). For all AGN feedback, gas is ejected in a bipolar fashion, parallel to the angular momentum vector of the gas in the BH kernel. Accompanying the AGN jets, that reach maximum allowed speeds, is an X-ray feedback mode that injects energy into the immediate surroundings of the BH. This additional feedback mode is added to capture the local effects of AGN jets since, due to resolution limitations, the AGN jets are temporarily hydrodynamically-decoupled. For more details on Simba, we refer the reader to Davé et al. (2019).

The flagship simulation has a comoving box length of 100 Mpc/ $h$  and an initial gas element mass resolution of  $1.82 \times 10^7 M_\odot$ . We also analyze a set of 50 Mpc/ $h$  boxes with mass resolution  $2.28 \times 10^6 M_\odot$  that toggles the galactic feedback modes on and off. Of these smaller boxes, we analyze four simulations: a stellar feedback only simulation ('SW only'), one that adds in radiative AGN feedback ('SW + Rad'), one that adds in AGN jets ('SW + Rad + Jet'), and a simulation with the fiducial feedback implementation ('Fiducial').

### 2.3. The CAMELS Simulations

The Cosmology and Astrophysics with MachinE Learning Simulations (CAMELS) project consists of thousands of N-body and state-of-the-art hydrodynamic simulations that span a vast cosmological and astrophysical parameter space (Villaescusa-Navarro et al. 2021, 2023). Each simulation is run with  $256^3$  gas particles in a box with co-moving side length 25 Mpc/ $h$  and an initial mass resolution of  $1.27 \times 10^7 M_\odot h$ . For this work, we analyze the simulations run with the IllustrisTNG and Simba models, which all use the same cosmological parameters:  $\Omega_m = 0.3$ ,  $\Omega_b = 0.049$ ,  $H_0 = 67.11$  km/s/Mpc,  $\sigma_8 = 0.8$ ,  $M_\nu = 0$  eV,  $w = -1$ , and  $n_s = 0.9624$ .

The CAMELS-Simba and CAMELS-TNG simulation suites feature 28 parameter variations that explore both galaxy formation and cosmology (Ni et al. 2023). Of these 28 parameters, 23 control the stellar modeling, SMBH modeling, and the implemented galactic feedback. These variations allow for an in depth exploration of which subgrid models can impact the predicted BHMF and, in turn, the GWB.

The CAMELS project includes a set of simulations, referred to as the 1P set, that vary parameters one at a

time while keeping all other aspects identical, including the initial conditions. We analyze the 1P set to determine which subgrid physics plays a role in setting the predicted GWB. The 23 astrophysics parameters that are explored herein are summarized for the IllustrisTNG suite in Table 1 and for the Simba suite in Table 2. Also included in the CAMELS project is a set of 27 simulations that are run with identical physics and cosmology but with varying initial conditions, referred to as the CV set. We analyze the CV set, alongside our box size analysis, to examine the impact of cosmic variance on the predicted GWB.

Larger box simulations are preferred for studying the GWB since convergence at the high mass end of the BHMF requires sufficient sampling of high mass halos, however larger box simulations are also more expensive to run. The benefit of having a large number of smaller box simulations through the CAMELS project is that we can isolate and explore the impact of individual astrophysics parameters by comparing simulations that vary only that parameter. Determining what physics has an impact can motivate future works to explore those effects in larger box simulations where the high mass end of the BHMF is more robust. Figure 1 illustrates this idea and also summarizes the pipeline we use to calculate the predicted GWB amplitude for a simulation using its BHMF.

#### 2.4. Calculating the BHMF

We calculate the BHMF by binning the SMBHs in each simulation into 0.2 dex bins. The BHMFs are calculated for discrete redshift snapshots from  $z = 0$  to  $z = 2$ . These differential number densities,  $\Phi(M_{\text{BH}}, z)$ , are then used directly in Eq. (4) to account for the redshift evolution of the population. For the CAMELS-TNG and CAMELS-Simba simulations, we pull the SMBH population from 23 different snapshots in the redshift range of interest. For the Simba simulations we similarly pull the SMBH data from 23 different snapshots that were chosen to match the CAMELS redshifts. For IllustrisTNG and MillenniumTNG the SMBH populations are instead pulled from the subhalo catalogs. How the BHMFs predicted by the simulations are used in the calculation of the GWB amplitude is described in the next section.

### 3. QUASAR-BASED GWB MODEL

We adopt the SMBHB population framework of Casey-Clyde et al. (2022) to transform simulation-predicted BHMFs into a GWB signal. In this approach, the empirically measured QLF is used as a tracer of the SMBHB population. This QLF-based model leverages

observed quasar demographics to constrain the mass distribution of SMBHBs and predict the GWB amplitude.

Casey-Clyde et al. (2022) computed the expected GWB, assuming that quasars are initially triggered by galaxy mergers. They found that for the model to reproduce the NANOGrav signal, the binary population must be approximately four times larger than the quasar population, implying a duty cycle where  $\sim 25\%$  of binaries are hosted by quasars. By calibrating our simulated BHMF against this observed quasar population, we can utilize the framework in Casey-Clyde et al. (2022, 2025) to obtain a self-consistent estimate of the GWB strain.

The transformation from the BHMF, from the cosmological simulations, to the BH Binary Mass Function (BHBMF) required for the GWB calculation proceeds in three steps: (1) isolating the active quasar population, (2) scaling to the total binary population, and (3) assigning secondary masses.

First, we treat the total BHMF from the simulation,  $\phi_{\text{sim}}(M_{\text{BH}}, z)$ , as the parent population. We derive the subset of these black holes that would appear as active quasars,  $\phi_{Q,\text{sim}}$ , by convolving the parent mass function with an Eddington Ratio Distribution Function (ERDF),  $P(\lambda)$ . The ERDF effectively acts as a duty cycle, quantifying the probability that a black hole of mass  $M_{\text{BH}}$  is accreting at Eddington ratio  $\lambda = L_{\text{bol}}/L_{\text{Edd}}$ . The number density of simulated quasars is therefore:

$$\frac{d^2\Phi_{Q,\text{sim}}}{dM_{\text{BH}} dz} = \frac{d^2\Phi_{\text{sim}}}{dM_{\text{BH}} dz} \times \int_{\lambda_{\text{min}}}^{\lambda_{\text{max}}} P(\lambda) d\lambda, \quad (1)$$

where the integral represents the duty cycle  $f_{\text{duty}}(M_{\text{BH}}, z)$ , or the fraction of black holes that are radiatively active (Casey-Clyde et al. 2025).

We then convert this active population into a binary population. Following the calibration in Casey-Clyde et al. (2022), we scale the active quasar population by a normalization factor  $\mathcal{N}_{\text{cal}} \approx 4$ , reflecting the observational constraint that there are roughly four times as many binaries as there are visible quasars. This is a model-inferred calibration factor derived from fitting quasar-based models to GWB limits (Casey-Clyde et al. 2022), rather than a direct observational constraint.

The primary mass distribution of the binaries is therefore:

$$\frac{d^2\Phi_{\text{BHB}}}{dM_{\text{BH},1} dz} \approx \mathcal{N}_{\text{cal}} \times \frac{d^2\Phi_{Q,\text{sim}}}{dM_{\text{BH},1} dz}. \quad (2)$$

Finally, because we do not explicitly track binary pairings, we assign a secondary mass  $M_{\text{BH},2}$  to each primary  $M_{\text{BH},1}$  by sampling a mass ratio  $q = M_{\text{BH},2}/M_{\text{BH},1}$ . The full differential SMBHB number density is given by:

$$\frac{d^3\Phi_{\text{BHB}}}{dM_{\text{BH},1} dq dz} \propto \left( \mathcal{N}_{\text{cal}} \frac{d^2\Phi_{Q,\text{sim}}}{dM_{\text{BH},1} dz} \right) p(q), \quad (3)$$

where  $p(q)$  is the SMBHB mass-ratio distribution, which we take as a log-normal centered at  $q = 0.33$  with width 0.5 dex. We adopt this distribution to remain consistent with the calibration of  $\mathcal{N}_{\text{cal}}$  in [Casey-Clyde et al. \(2022\)](#), though we acknowledge that theoretical models often predict log-uniform distributions favoring lower mass ratios.

Here  $p(q)$  determines only the secondary mass; the primary mass  $M_{\text{BH},1}$  is drawn directly from the simulation’s feedback-regulated BHMF.

The characteristic strain spectrum  $h_c(f)$  of the GWB is obtained by integrating over this derived binary population:

$$h_c^2(f) = \iint \frac{1}{1+z} \frac{d^3\Phi_{\text{BHB}}}{dM_{\text{BH},1} dq dz} \frac{dE_{\text{gw}}}{d \ln f_r} dM_{\text{BH},1} dq dz, \quad (4)$$

where the term  $dE_{\text{gw}}/d \ln f_r$  is the GW energy emitted per logarithmic frequency interval. For circular binaries, the GW energy spectrum is ([Phinney 2001](#)):

$$\frac{dE_{\text{gw}}}{d \ln f_r} = \frac{\pi^{2/3}}{3} \mathcal{M}^{5/3} f_r^{2/3}, \quad (5)$$

where  $\mathcal{M} = M_{\text{BH},1} q^{3/5} (1+q)^{-1/5}$  is the chirp mass and  $f_r = f(1+z)$  is the rest-frame frequency. In this work, we insert the BHMFs predicted by cosmological simulations ( $\Phi_{\text{sim}}$ ) into this framework, thereby mapping theoretical SMBHB growth models directly to the GWB amplitude.

Finally, we calculate the characteristic strain assuming a power-law spectrum  $h_c(f) \propto f^{-2/3}$  ([Phinney 2001](#)). This approximation implicitly neglects environmental hardening mechanisms (e.g., stellar scattering) that may flatten the spectrum at low frequencies, as well as the finite number of sources that introduces anisotropies at high frequencies. We use this power law to report the characteristic GWB amplitude ( $A_{\text{GWB}}$ ) at a standard reference frequency of  $f = 1 \text{ yr}^{-1}$ .

## 4. RESULTS

Here we discuss the resulting BH mass functions and predicted GWB amplitudes from the IllustrisTNG, MillenniumTNG, Simba, and CAMELS simulations.

### 4.1. AGN Feedback and the Black Hole Mass Function

We first demonstrate the impact of altering AGN feedback on the BHMF. Using the Simba AGN feedback variation 50 Mpc/h side length boxes, we compute the BHMF in four simulations: a stellar feedback only simulation (‘SW only’), one that adds in radiative AGN feedback (‘SW + Rad’), one that adds in AGN jets (‘SW + Rad + Jet’), and a simulation with the fiducial feedback implementation (‘Fiducial’). Figure 2 shows the

predicted BHMF at  $z = 0$  from these simulations to illustrate how much the mass function can vary given different galactic feedback implementations, motivating further exploration of this effect. The Simba fiducial model (black line) predicts significantly fewer massive black holes that would fall in the PTA band than the other models, which remove different aspects of the AGN feedback model. Removing some or all aspects of the AGN feedback (colored dashed/dotted lines in Figure 2) results in more high-mass black holes, and, as shown in many previous works, produces simulations with unrealistic galaxy properties and intergalactic medium properties ([Christiansen et al. 2020; Tillman et al. 2023, 2025](#)).

### 4.2. The SMBH mass function and convergence

For each BHMF plot, we highlight the  $M_{\text{BH}} \geq 10^8 M_{\odot}$  mass range since it is the most relevant for predictions of the GWB amplitude. However, even within this range the higher mass BHs will contribute more to the predicted amplitude. We calculate the BHMF for different box sizes and present them in Figure 3. We plot the BHMF integrated over  $z = 0 - 2$  since the GWB amplitude calculation integrates over the SMBHB population in this redshift range. We also mark where mass bins have fewer than 10 SMBHBs with a horizontal dashed line that match the color of the corresponding simulation. Below the dashed line, the BHMF will be dominated by Poisson noise. The left plot shows results for IllustrisTNG and MillenniumTNG while the right plot shows results for Simba. Figure 3 also shows the median predicted mass function and the 16th-to-84th percentiles for the CAMELS-TNG and CAMELS-Simba CV sets. For our purposes, we consider the BHMF of a simulation to be converged if the difference from the largest box simulation (MillenniumTNG and Simba 100 Mpc/h) is within the range expected due to cosmic variance (the  $2\sigma$  range from the CAMELS CV sets).

For the IllustrisTNG and MillenniumTNG simulations, we find that the BH mass functions are converged within 0.5 dex for the simulations with co-moving box lengths of at least 35 Mpc/h at masses  $M_{\text{BH}} > 10^8 M_{\odot}$ . At  $M_{\text{BH}} > 10^9 M_{\odot}$ , the variation between these different box size simulations is within the expected range due to cosmic variance, calculated from the CAMELS-TNG CV set, and is therefore considered converged. Convergence at this mass range is important as higher mass SMBHBs will dominate the predicted amplitude. At masses below  $M_{\text{BH}} = 10^8 M_{\odot}$  the mass function shows variance of up to a dex between simulations. The large variation in the mass function at these masses is likely due to resolution differences between the simulations

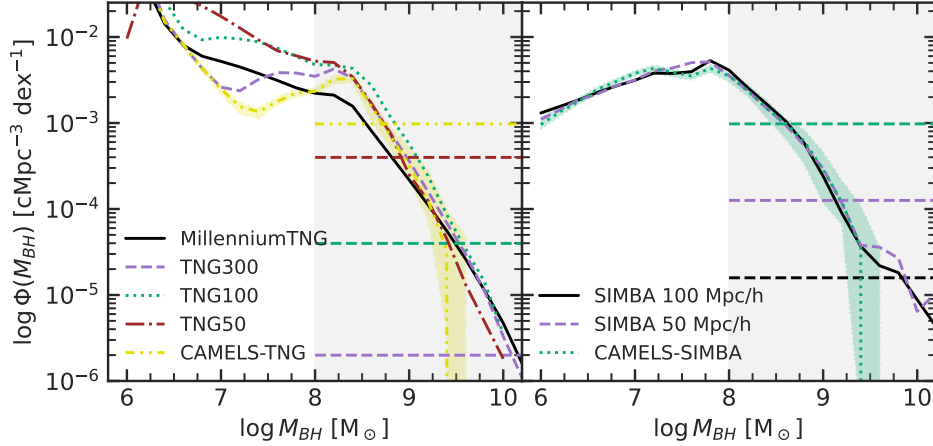


**Figure 3.** The BHMF (integrated from  $z = 0$  to 2) predicted by the IllustrisTNG (left) and Simba (right) simulations for different box sizes. MillenniumTNG, TNG300, TNG100, TNG50, and CAMELS-TNG/Simba are run in a box with co-moving side length 500, 205, 75, 35, and 25 Mpc/h respectively. The Simba simulations are run in a box with co-moving side length as labeled in the legend. The dashed horizontal line corresponds to where mass bins contain fewer than 10 SMBHs matched to the simulations by color. Both simulation models struggle to produce a well sampled high mass ( $M_{BH} > 10^9 M_{\odot}$ ) BHMF in a box with side length 25 Mpc/h, i.e. in the CAMELS simulations. These results imply that a box size length of at least 35 Mpc/h for IllustrisTNG and 50 Mpc/h for Simba is required to produce a reasonable sampled BHMF for  $M_{BH} > 10^9 M_{\odot}$ . For the CAMELS simulations, the shaded region corresponds to the 16th-to-84th percentiles from the CV set.

and will have minimal to no impact on the predicted GWB amplitude.

The Simba simulations show significant ( $< 0.1$  dex) agreement between the three different box size simulations up to  $M_{BH} = 10^{9.5} M_{\odot}$ . The BHMFs vary more between box sizes at the high mass end ( $M_{BH} \gtrsim 10^{9.5} M_{\odot}$ ) due to under sampling of massive halos in small boxes. However, the variation between the simulations is within the range expected due to cosmic variance calculated from the CAMELS-Simba CV set and is therefore considered converged.

Although both CAMELS-TNG and CAMELS-Simba fail to produce SMBHs in mass bins larger than  $M_{BH} \sim 10^{9.5} M_{\odot}$ , the variation between the larger box size simulations is less than the variation expected from the CAMELS CV sets at lower mass bins. These results imply that a box size of at least  $(35 \text{ Mpc/h})^3$  for IllustrisTNG or  $(50 \text{ Mpc/h})^3$  for Simba is required for convergence of the BHMF.

IllustrisTNG and Simba vary dramatically in shape at the low mass ( $M_{BH} \lesssim 10^8 M_{\odot}$ ) end of the BHMF. The IllustrisTNG BHMF rises towards lower masses while the Simba BHMF turns over at these same masses. This is a result in the difference in how seeding is modeled in the two simulations. Since in Simba, BHs are seeded at higher host masses, there will be many less SMBHs at the low mass end than there are in IllustrisTNG which produces the differences seen between their BHMFs.

Figures 4 and 5 show the predicted BH mass functions for the CAMELS-TNG and CAMELS-Simba 1P simu-

lation sets respectively. For each parameter, the mass function is calculated five times for different values of that parameter for which the range of values chosen are discussed in Tables 1 and 2 in the Appendix. The parameter being varied is labeled in the top right corner in each plot. Not every parameter variation produces changes in the BHMF that will impact the predicted GWB amplitude. For example, in Figure 5,  $A_{\text{AGN}2}$  has minimal impact on the mass function across the full mass range while  $\text{WindColdTemp}$  largely impacts the mass function at  $M_{BH} < 10^8 M_{\odot}$ . In both cases, the impact on the predicted GWB amplitude will be low. For both CAMELS-TNG and CAMELS-Simba, many mass functions appear noisy at the highest masses ( $M_{BH} \sim 10^9 M_{\odot}$ ) due to lack of convergence in the small simulation box.

For both CAMELS-TNG and CAMELS-Simba, the high mass end of the BHMF ( $M_{BH} \geq 10^8 M_{\odot}$ ) is impacted by a mix of stellar and AGN parameters. For CAMELS-TNG, only  $A_{\text{BHseed}}$  has an impact on the low mass end of the BHMF ( $M_{BH} < 10^7 M_{\odot}$ ). This is in contrast to CAMELS-Simba where many parameters, both stellar and AGN, impact the low mass end of the BHMF. Changes to the low mass end of the BHMF will not impact the predicted GWB amplitude but could have implications for other GWB metrics. We discuss how these different parameters affect the predicted BHMF and thus the GWB amplitude in Section 5.2.

#### 4.3. The GWB amplitude

#### 4.3.1. The predicted GWB amplitude In Flagship Models

Figure 6 shows the predicted GWB amplitude for the different box size simulations and the CAMELS CV sets for both IllustrisTNG and Simba. The figure also shows the predicted GWB amplitude for the feedback variant Simba simulations. The two smaller points in each figure, at  $25 \text{ Mpc}/h$ , represent the 16th-to-84th percentile ( $\sim 2\sigma$ ) variation predicted by the CAMELS CV set. Also included is the NANOGrav 15-yr dataset measurement of the GWB amplitude and a shaded region representing the error (Agazie et al. 2023). The simulation model that the prediction is from is labeled in the legend.

Simulation predicted values of  $A_{\text{GWB}}$  converge beyond  $35 \text{ Mpc}/h$  for MillenniumTNG/IllustrisTNG and  $50 \text{ Mpc}/h$  for Simba within the variance of what is expected from cosmic variance (CAMELS 25  $\text{Mpc}/h$  CV set simulations). Importantly all fiducial simulations across a range of volumes (black points) consistently under-predict the GWB amplitude when compared to the measured value from NANOGrav. In our framework, this implies they are missing massive black holes within the  $z < 2$  redshift range we investigate.

We note exception in the Simba runs without AGN feedback or certain modes of AGN feedback. In particular the Simba SW + Rad and SW only feedback variant simulations, which both correspond to the removal of the AGN feedback jet mode, match the observed GWB. Recall in the previous section these simulations produced more black holes in the high mass end, explaining this result (see Figure 2). In particular, this is a result of the differences seen in the BHMF at  $M_{BH} > 10^9 M_{\odot}$ , highlighting the significant contribution that the highest BH masses have on the predicted amplitude.

While Simba SW + Rad and SW only feedback variant simulations produce the correct GWB amplitude within the (Casey-Clyde et al. 2022, 2025) framework, they dramatically fail in producing realistic galaxy populations since the jet mode is responsible for quenching (Dave et al. 2019; Christiansen et al. 2020). The failure of all models in producing both realistic galaxies and the correct amplitude of the GWB points to a need to revise black hole seeding and growth models in cosmological simulations. This points to an agreement between the GWB amplitude and recent JWST results suggesting that black holes are seeded early and perhaps grew much faster than their host galaxies in the early universe, which is not modeled in these simulations (see Pacucci et al. 2023, and references therein).

#### 4.3.2. CAMELS Parameter Variation GWB Amplitude

Figure 7 shows the predicted GWB amplitude values from the CAMELS-TNG and CAMELS-Simba 1P sets. Descriptions of these parameter variations can be found in Tables 1 and 2. We order the parameters in these plots from the highest impact on the predicted GWB amplitude on the left side to the lowest impact towards the right side. For each simulation, only one parameter produces a large enough change in the predicted GWB amplitude to reproduce the measured value,  $\beta$  for CAMELS-TNG and  $A_{\text{BHseed}}$  for CAMELS-Simba. However, we refrain from comparing these predictions to the measured background for two reasons. One is the lack of convergence in the CAMELS simulations due to the small box size. Second is that variations due to the highest and lowest parameter values in the CAMELS 1P set often produce non-physical results such as a mismatch between the observed and predicted stellar mass function. Due to these facts, this analysis serves purely to analyze the extent to which galactic feedback may impact the predicted GWB amplitude. These results also emphasize that even when varying these parameters to extreme values, these simulations still struggle to reproduce the measured amplitude. For a robust comparison with observations, the simulations must be run in a larger box and furthermore confirmed to reproduce realistic galaxies given the different parameter variations.

## 5. DISCUSSION

### 5.1. Implications for Massive Black Hole Growth

The fiducial IllustrisTNG, MillenniumTNG, and Simba simulation models all under-predict the observed GWB amplitude using the quasar framework. This comes from a lack of SMBHs populating the highest mass range ( $M_{BH} \geq 10^8 M_{\odot}$ ) as seen through the BHMF. Some simulations with varying feedback prescriptions predict a GWB amplitude that matches what is measured via PTAs. However, those variations are unrealistic as they do not include or suppress mechanisms that regulate SMBH growth and as a result those simulations do not reproduce other galaxy properties. Instead, we can examine those simulations to determine the number of SMBHs that would be required by the fiducial models to resolve simulation predictions and PTA measurement of the GWB amplitude. The CAMELS 1P set simulations are not converged at the highest mass ranges of the BHMF so we conduct this exercise with the Simba feedback variant simulations which are converged with a box length of  $50 \text{ Mpc}/h$ . The SW only and the SW + Rad simulations match the measured GWB amplitude.

We will look specifically at the SW + Rad simulation as it is more realistic including both stellar feedback and a form of AGN feedback. Looking at how many

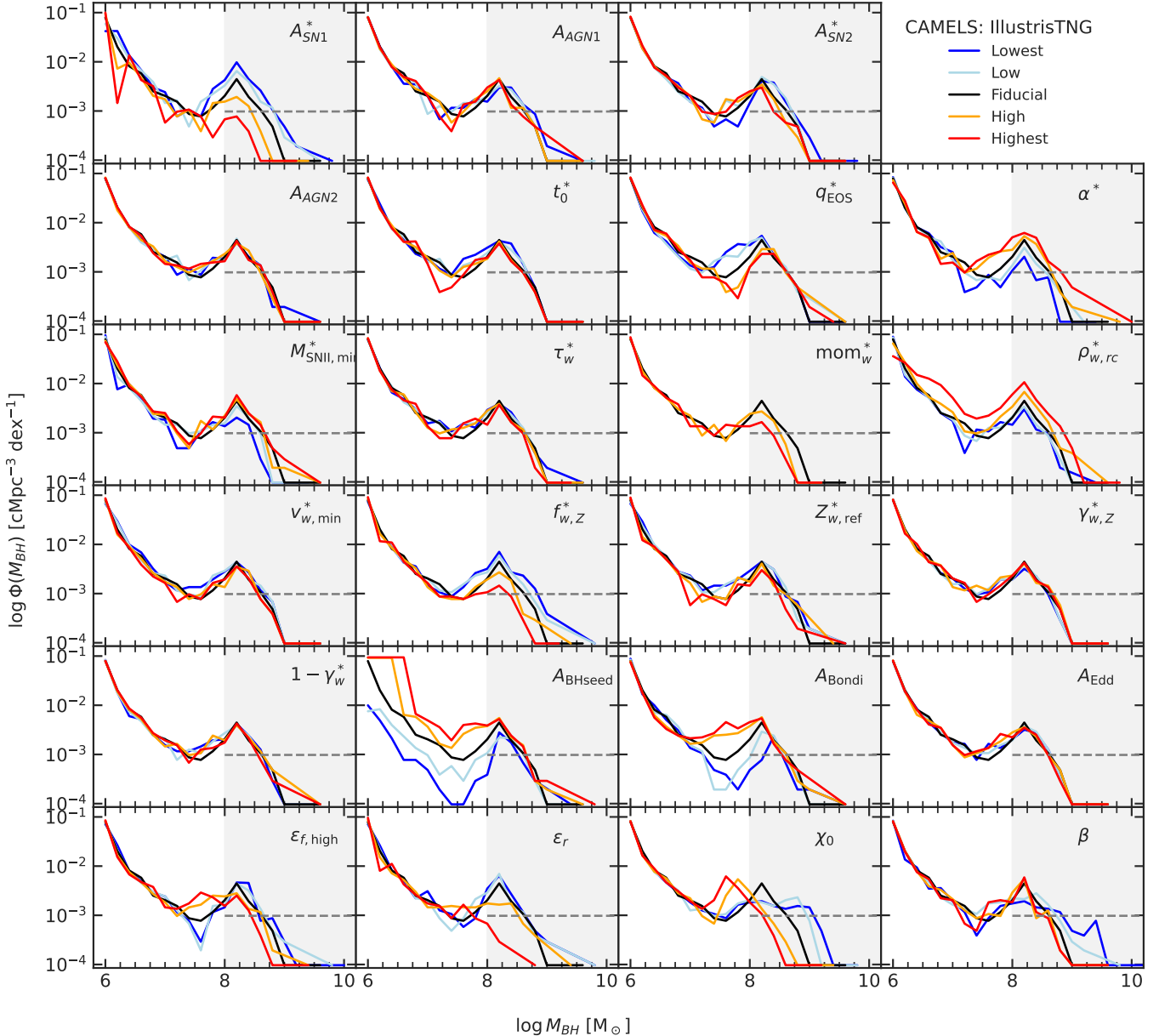


**Figure 4.** The predicted BHMF at  $z = 0$  from the CAMELS-TNG simulation 1P set for parameter variations controlling galactic feedback. The name of the parameter varied is labeled in the top right of each plot. The legend indicates what color corresponds to the parameter value with red and blue being the largest and smallest value respectively. The grey dashed line marks where the mass bins contain fewer than 10 SMBHs. Some galactic feedback parameters produce large variations in the predicted BHMF while others have minimal effect. Changes to the high mass end of the BHMF are expected to impact the predicted GWB amplitude while changes to the low mass end are not. Descriptions of the parameters can be found in Table 1.

more SMBHs this simulation has in different mass bins when compared to the fiducial 50 Mpc/h Simba box will demonstrate to what degree the most massive SMBHs are under-predicted in the fiducial Simba model. For the mass bin of  $10^8 < M_{BH} < 10^{8.5} M_{\odot}$ , the SW + Rad simulation has  $\sim 1.5$  times as many SMBHs as the fiducial case. For  $10^{8.5} < M_{BH} < 10^9 M_{\odot}$  the SW + Rad simulations has  $\sim 2.5$  times as many SMBHs, for

$10^9 < M_{BH} < 10^{9.5} M_{\odot}$  there are  $\sim 5.5$  times as many SMBHs, and for  $M_{BH} > 10^{9.5} M_{\odot}$  there are  $\sim 3.5$  times as many SMBHs.

Overall, the fiducial Simba simulation requires  $\sim 1.5$  to  $5.5$  times more of the most massive SMBHs ( $M_{BH} > 10^8 M_{\odot}$ ), depending on the mass bin, to reproduce the measured GWB amplitude value. Since the higher mass BHs contribute more to the GWB amplitude,

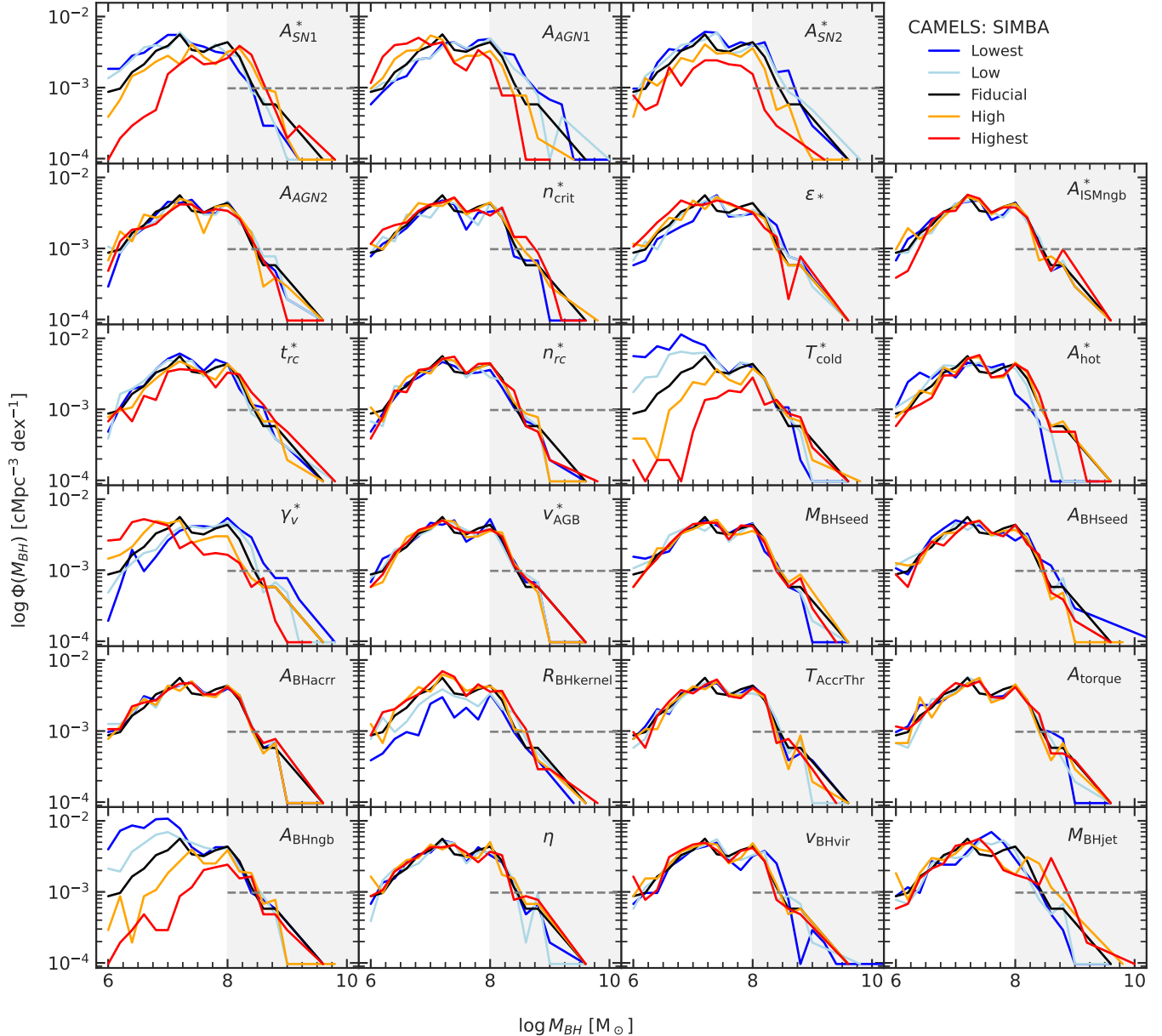


**Figure 5.** The same as Figure 4 but for the CAMELS-Simba simulation suite. Descriptions of the parameters can be found in Table 2.

a similar amplitude can be predicted with, for example, less  $M_{BH} > 10^{9.5} M_{\odot}$  BHs if there are even more  $M_{BH} < 10^{9.5} M_{\odot}$  BHs. However, those lower mass BHs are less impactful in their contribution to the GWB, so many more are required. When utilizing the local SMBH population to calculate the GWB amplitude, Sato-Polito & Zaldarriaga (2025) similarly found that more SMBHs were necessary, requiring 10 times more SMBHs than local measurements suggests to reproduce the measured amplitude SMBHs. They found that SMBHs with masses  $M_{BH} \gtrsim 10^{10} M_{\odot}$  contributed the most, but that current amplitude measurements dis-

favors a BHMF that is dominated by a few very heavy sources. Furthermore, Mingarelli (2026) found that one requires these very massive  $10^{10} M_{\odot}$  SMBH binaries to create the GWB measured by PTAs, using simple conservation of energy arguments. These results highlight the need to re-evaluate current models for SMBH growth and seeding to determine how to grow these missing massive SMBHs in state-of-the-art cosmological hydrodynamic simulations. However, we emphasize that missing massive SMBHs is not the only possible explanation for the deficit. The GWB amplitude is degenerate with the binary merger rate; a higher binary duty cycle than

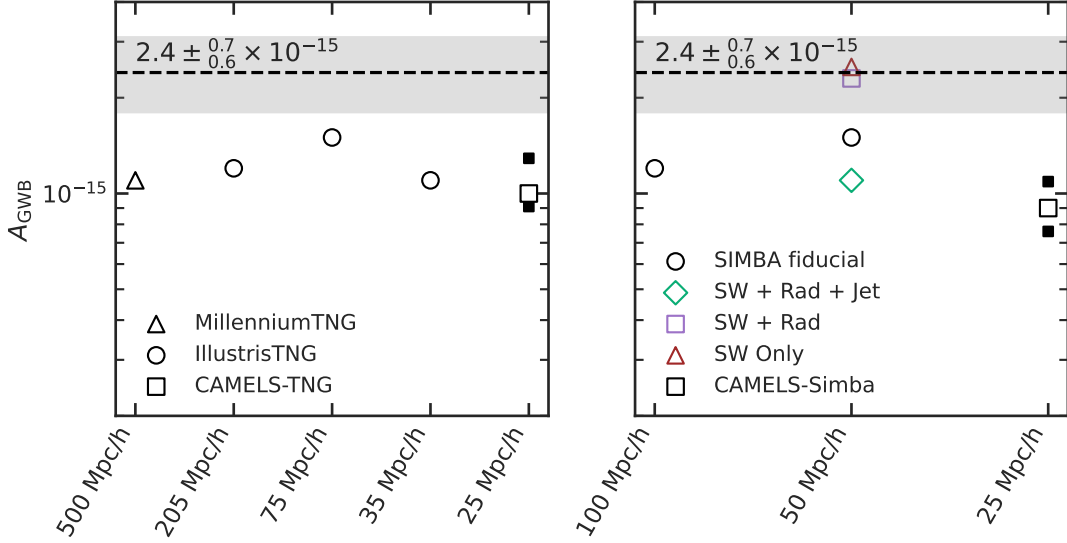


**Figure 6.** The predicted GWB amplitude for the (left) IllustrisTNG and MillenniumTNG simulations and (right) Simba simulations. The legend denotes which simulation model the predicted amplitude is from and the x-axis denotes the simulation box side-length. The two smaller shaded points for the 25 Mpc/h simulation represents the 16th-to-84th percentiles calculated from the CAMELS CV set. The dashed horizontal line and shaded region corresponds to the measured GWB amplitude from the NANOGrav 15 year dataset.

inferred by our  $\mathcal{N}_{cal}$  calibration could similarly boost the signal. Additionally, deviations from the assumed  $-2/3$  spectral index could alter the extrapolated amplitude at  $f = 1 \text{ yr}^{-1}$ .

### 5.2. Stellar and AGN feedback and the GWB Amplitude

The link between the GWB amplitude, the binary massive black hole population and, in turn, the massive black hole population provides an important test for galaxy formation models, since the high-mass BHMF is shaped by feedback physics that governs black hole growth and additionally to the black hole seeding prescription at high redshift.

Our results demonstrate that the choice of feedback model (including both AGN and stellar/SNe feedback) has a strong impact on the BHMF in cosmological box simulations and hence the predicted GWB amplitude using the quasar framework. In simulations with inefficient AGN or stellar feedback, SMBHs can grow rapidly in massive halos, yielding an overabundance of extremely massive black holes (e.g.,  $M_{BH} \gtrsim 10^9\text{--}10^{10} M_{\odot}$ ). Such models predict a significantly higher GWB amplitude than models with strong feedback. In contrast, when energetic AGN and/or SNe feedback is included, it self-regulates black hole accretion in large halos and curtails the growth of the most massive black holes. This produces a cut-off or flattening in the BHMF at the high-mass end, which in turn lowers the GWB amplitude.

Our findings on the BHMF are consistent with previous studies on the behavior of BH growth in cosmological simulations. Large-volume simulations of galaxy formation, such as Illustris, EAGLE, IllustrisTNG, and Simba, all require some form of AGN feedback to reproduce galaxy and star formation properties, but they differ in the details of BH growth outcomes. For example, the original Illustris simulation (which employed thermal bubble AGN feedback) yielded very massive BHs in group and cluster-scale halos, overshooting some observational constraints on BH masses (Sijacki et al. 2015). The IllustrisTNG model introduced a kinetic AGN feedback mode that more efficiently quenches massive galaxies, thereby slowing down BH growth at late times (Weinberger et al. 2018; Pillepich et al. 2018). As a result, IllustrisTNG produces fewer ultra-massive black holes at  $z = 0$  than Illustris. The EAGLE simulation, which calibrates AGN heating to reproduce the  $M_{\bullet}\text{--}\sigma$  relation, similarly finds that strong AGN feedback is needed to prevent excessive BH buildup in the most massive galaxies (Schaye et al. 2015; Rosas-Guevara et al. 2015; McAlpine et al. 2018). By contrast, if AGN feedback is turned off or greatly weakened (leaving only stellar feedback), simulations tend to produce overly massive central BHs.

Using the Simba simulation as an illustrative case: our tests show that removing kinetic AGN jet feedback leads to a factor of a few increase in the number density of  $M_{\bullet} > 10^8 M_{\odot}$  black holes (relative to the fiducial Simba model with jets), and completely turning off all

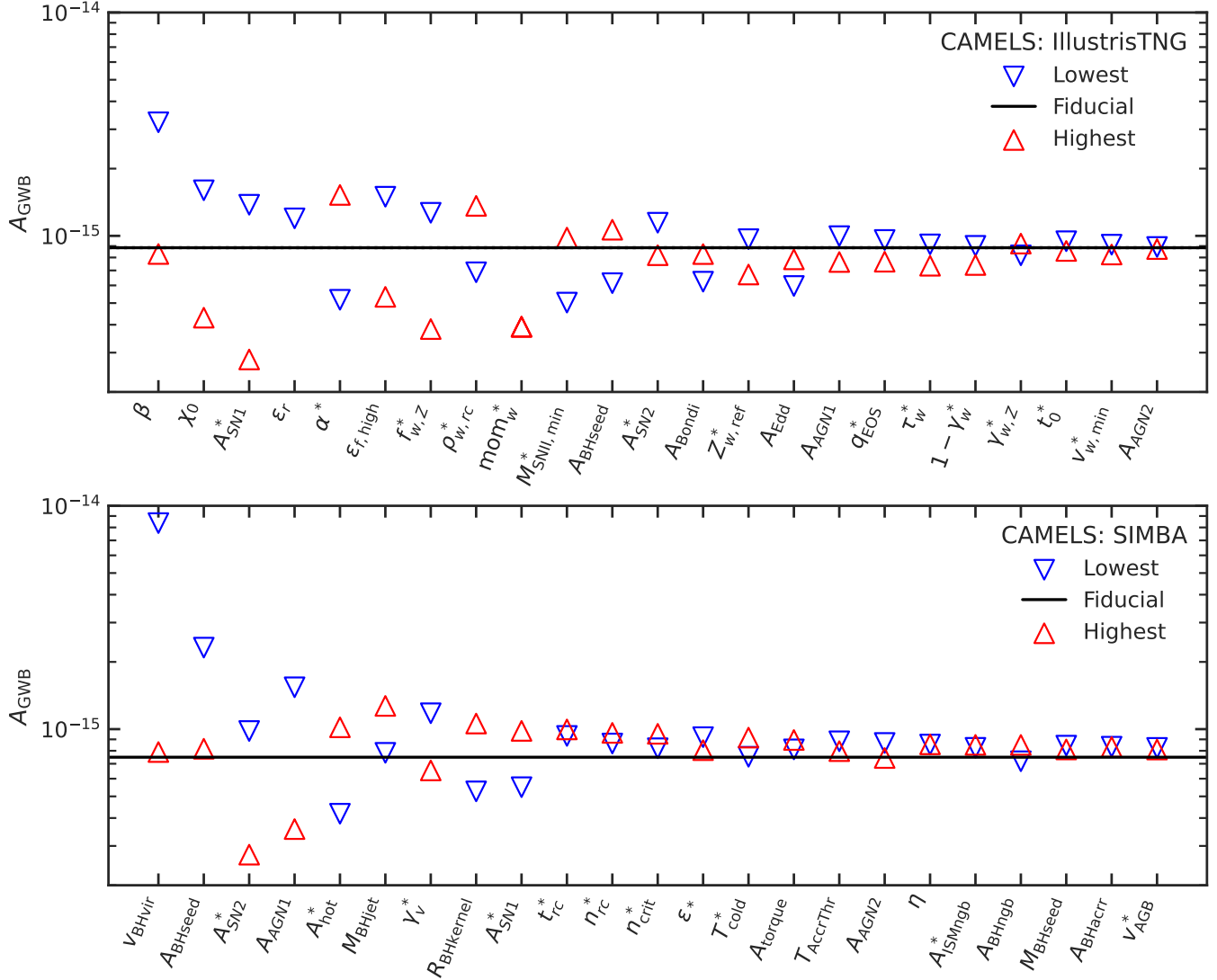


**Figure 7.** The predicted GWB amplitude from the CAMELS-TNG (top) and CAMELS-Simba (bottom) simulation 1P set for parameter variations controlling galactic feedback. The parameter varied is labeled on the x-axis. Triangles pointing up (red) are for increases in parameter value while triangles pointed down (blue) are for decreases in parameter value. The intermediate parameter values are not plotted but lie between the minimum/maximum and fiducial for all cases. The black solid horizontal line corresponds to the fiducial simulation prediction.

AGN feedback causes an even more dramatic upturn in the high-mass BHMF. Such variations in the high-mass tail of the BHMF translate almost directly into GWB amplitude differences. The right plot of Figure 6 of our results (see above) explicitly demonstrated that models with no AGN or reduced feedback yield a substantially higher background strain than those with efficient AGN feedback, owing to the surplus of massive BH binaries in the former case.

We see this demonstrated in Figure 7 with the most impactful parameters for the GWB amplitude being  $\beta$  and  $\chi_0$  for IllustrisTNG and  $v_{BHvir}$  for Simba. These parameters directly control the strength of the differ-

ent AGN feedback models implemented in the simulations. This demonstrates the capabilities for AGN feedback to create a self-regulating effect on SMBH growth. The next most impactful parameter on the GWB amplitude for Simba is  $A_{BHseed}$ , which more directly impacts the BHMF by controlling the mass at which SMBHs are seeded. While some of these variations predict a higher background strain that better matches the measured value from PTAs, these extreme feedback scenarios are already ruled out through their inability to reproduce observed galaxy statistics. Therefore, we demonstrate that PTA observations should provide constraints on the BHMF in terms of seeding and growth models.

It is worth noting that while many stellar feedback parameters primarily affect the low-mass end of the BHMF—for instance, stronger SN-driven winds can delay BH seed growth in galaxies (Dubois et al. 2015; Anglés-Alcázar et al. 2017; Ravi et al. 2019), our analysis shows that some stellar feedback parameters can, in fact, influence the predicted gravitational wave background. In particular, in the Simba suite we find that the normalization factor for the speed of galactic winds ( $A_{\text{SN2}}^*$ ) and the fraction of wind particles ejected in the hot phase ( $A_{\text{hot}}^*$ ) significantly affect the resulting GWB amplitude. In the IllustrisTNG simulations, the most important stellar feedback parameters are the normalization factor for the energy in galactic winds per unit star formation ( $A_{\text{SN1}}^*$ ) and the power-law index of the stellar initial mass function above  $1 M_\odot$  ( $\alpha^*$ ). For both Simba and IllustrisTNG parameters affect how efficiently stellar-driven outflows regulate black hole growth, and thus indirectly shape the abundance of SMBHs in the PTA-sensitive mass range. Moreover, our framework relies on quasars as tracers for the binary population. Consequently, AGN feedback plays a dual role in our predictions: it physically limits the black hole mass (shaping the BHMF) and, by suppressing accretion rates, effectively reduces the number of visible tracers used to infer the binary population. This double suppression implies that strong feedback models may underestimate the GWB if a significant population of dark binaries exists in quenched galaxies.

### 5.3. Assumptions in modeling

Our approach makes several simplifying assumptions in mapping the simulated BH mass function to a predicted GWB amplitude.

First, we assume that the instantaneous BHMF from the simulations directly represents the population of SMBHs participating in binaries that contribute to the nanohertz GWB. This implicitly neglects details of merger timing, binary pairing efficiency, and environmental hardening processes that depend on each galaxy’s dynamical history. Since binary evolution occurs on Gyr timescales, the GWB amplitude is dominated by systems assumed at higher redshifts. However, the impact of time delays on the amplitude is complex. While long delays can prevent binaries from merging by  $z = 0$ , thereby suppressing the signal, they also shift the merger epoch of high-redshift binaries to lower redshifts. Since the GW strain scales as  $1/d_L$ , binaries merging at lower redshift have a larger strain. Therefore, accounting for time delays could either suppress or enhance the predicted amplitude by shifting mergers to the local Universe, depending on the specific delay time distribution.

Second, we assume that the empirical relation between quasar luminosity and BH mass can be used to weight the simulated BHMF via the quasar luminosity function, effectively treating quasar activity as a tracer of binary incidence. This step assumes that all quasars of a given mass have equal likelihood of forming binaries, and that the redshift evolution of the quasar population mirrors that of SMBHs.

Third, we assume the empirical duty cycle to be constant across all models which neglects how the physical duty cycle in simulations, including the extreme feedback variations, diverge from that calibration. This mapping assumes that quasar visibility remains constant across all models.

Fourth, the model prescribes a lognormal mass-ratio distribution and circular binary orbits, omitting eccentricity evolution and spin coupling, both of which can alter the spectral shape and amplitude of the GWB.

Future work should compare our method here to those that couple simulation-derived BHMFs with self-consistent merger trees that explicitly track SMBH pairing, dynamical friction, and binary hardening within evolving galaxies. Incorporating such merger histories would allow us to directly compute the SMBHB formation rate and residence time at PTA frequencies, providing a more physically motivated connection between simulated BH growth and the observed GWB amplitude (e.g., Sesana 2013; Kelley et al. 2017b; Barausse et al. 2020; Chen et al. 2025). Previous work analyzing the Illustris simulation took care to include many of the environmental mechanisms expected to impact GWB predictions (dynamical friction, stellar ‘loss-cone’ scattering, viscous drag from a circumbinary disc, and eccentric binary evolution Kelley et al. 2017a,b) and found an amplitude of up to  $10^{-15}$  at a frequency of  $1 \text{ yr}^{-1}$ .

Even when considering these additional factors, despite the method use, all predictions reported from cosmological simulations under-predict the value reported by the NANOGrav 15-year dataset. Considering these additional environmental factors also seem to reduce the predicted amplitude rather than increase it, at least for Illustris. When calculating the amplitude predicted by Illustris with our model we find an amplitude of  $1.6 \times 10^{-15}$ , which is higher than that found by Kelley et al. (2017b). This is due to the fact that at the massive end of the BHMF, Illustris has more massive SMBHs than IllustrisTNG in the relevant redshift range. This comparison implies that it is important to consider these environmental mechanisms when calculating the GWB amplitude, but that the consideration of these mechanisms alone cannot resolve the tension between simulation predictions and PTA measurements.

Finally, works following this one should aim to establish a self-consistent framework for predicting the GWB amplitude from simulations which considers these environmental mechanisms and utilizes merger histories. A recent study built a framework for building gravitational wave event catalogs by assigning merger events to stellar particles in a simulation and applied it to MillenniumTNG (Marinacci et al. 2025). Follow-up studies could utilize such a tool for a more self-consistent analysis of the GWB in cosmological hydrodynamic simulations.

## 6. CONCLUSIONS

We have developed a framework that connects simulation-predicted SMBH mass functions to the GWB amplitude measured by PTAs. Building on the quasar-based population model of Casey-Clyde et al. (2022), we derive an estimate of the SMBHB population using the subset of SMBHs that would appear as active quasars. Casey-Clyde et al. (2025) found that a quarter of these will be in binary form. This then allows us to compute the GWB amplitude. We apply this framework to the IllustrisTNG, MillenniumTNG, Simba and CAMELS simulation suites spanning volumes from 25 to 500 Mpc/h and covering a range of astrophysical models.

Our main conclusions are as follows:

- We predict a value for the GWB amplitude ( $A_{\text{GWB}}$ ) at a reference frequency of 1 yr<sup>-1</sup> in various cosmological simulations. For IllustrisTNG and MillenniumTNG,  $A_{\text{GWB}}$  spans  $1.1 - 1.5 \times 10^{-15}$  for 35-500 Mpc/h boxes. For Simba  $A_{\text{GWB}}$  spans  $1.2 - 1.5 \times 10^{-15}$  for 50-100 Mpc/h boxes.
- The IllustrisTNG, MillenniumTNG, and Simba fiducial simulation models all under-predict the GWB strain amplitude by a factor of  $\sim 2$  and require 5.5 times more of the most massive SMBHs ( $M_{BH} > 10^9 M_{\odot}$ ) to reproduce the measured strain.
- Varying the underlying AGN and stellar feedback prescriptions produces systematic differences in both the shape and normalization of the BHMF. These differences can impact the predicted GWB strain amplitude by a factor of 2 for the Simba feedback variant simulations and up to a factor of 10 for CAMELS extreme feedback variations.
- The feedback parameters most critical to the high-mass end of the BHMF, and hence to the GWB amplitude, include, but are not limited to, the normalization of AGN feedback energy, the speed and

thermal fraction of stellar winds, and the high-mass slope of the stellar initial mass function. These parameters regulate SMBH growth in massive galaxies and thus control the abundance of binaries that dominate the PTA frequency band.

- We find convergence in the predicted GWB amplitude for volumes larger than  $\sim (35 - 50 \text{ Mpc}/h)^3$ . At  $(25 \text{ Mpc}/h)^3$  we find that cosmic variance results in a  $2\sigma$  deviation of  $\sim 0.1$  dex in the predicted GWB amplitude and significant noise in the BHMF for  $M_{BH} > 10^9 M_{\odot}$ , a mass range vitally important for predictions of the amplitude.

Comparison with PTA observations illuminates a new empirical constraint on SMBH growth and feedback physics in large scale simulations. Matching the GWB amplitude measured by PTAs requires simulations to produce realistic high-mass SMBH abundances consistent with both electromagnetic and GW observations. Two Simba feedback variant simulations and two CAMELS simulations were able to reproduce the expected signal by removing or heavily suppressing AGN and stellar feedback models. However, these simulations do not reproduce observed galactic statistics and are thus ruled out as physically realistic models. Therefore, SMBH growth and seeding models in cosmological hydrodynamic simulations likely need to be re-evaluated in order to determine how to effectively reproduce the necessary SMBH population.

While this work reported the GWB amplitude at a reference frequency of 1 yr<sup>-1</sup>, analyzing the amplitude at different frequencies or over the full characteristic strain spectrum could provide further insight into the impact that galactic feedback has on the GWB. This type of analysis would benefit more from the inclusion of environmental factors, such as binary hardening, merger timing, and pairing efficiency, as many of these processes are expected to impact the highest and lowest frequencies of the characteristic strain spectrum. Another factor to consider is the cosmological parameters implemented in these simulations. While we did not explore the impact of these assumptions, the CAMELS simulations do explore some variation in cosmological parameters such as  $\sigma_8$  and  $\Omega_m$ . Changes to dark matter or dark energy models could affect the growth of density perturbations which could propagate to affect early halo growth and SMBH seeding. Earlier SMBH seeding could give these objects more time to grow and relax the need for more extreme accretion scenarios.

This study establishes an empirical bridge between cosmological simulations, quasar demographics, and the GWB. Our framework assumes that the instantaneous

BHMF reflects the population of binary SMBHs and that quasar activity traces SMBHB incidence. These simplifying assumptions neglect merger timing, pairing efficiency, and binary hardening processes, which future work should incorporate using self-consistent merger tree modeling. Coupling simulation-based BHMFs with detailed binary evolution physics will enable a more predictive description of the GW Universe.

<sup>1</sup> B.B. acknowledges support from NASA grant  
<sup>2</sup> 80NSSC24K0773 (ATP-23- ATP23-0149) and NASA  
<sup>3</sup> grant No. 80NSSC20K0500. B.B. acknowledges NSF  
<sup>4</sup> grant AST-2407877. B.B. is grateful for the generous  
<sup>5</sup> support by the David and Lucile Packard Foundation  
<sup>6</sup> and the Alfred P. Sloan Foundation. B.B. thanks the  
<sup>7</sup> Center for Computational Astrophysics (CCA) of the  
<sup>8</sup> Flatiron Institute and the Mathematics and Physical  
<sup>9</sup> Sciences (MPS) division of the Simons Foundation for  
<sup>10</sup> support. The Flatiron Institute is supported by the  
<sup>11</sup> Simons Foundation. The authors thank Laura Blecha  
<sup>12</sup> for valuable comments. C.M.F.M. was supported in  
<sup>13</sup> part by the National Science Foundation under Grants  
<sup>14</sup> No. NSF PHY-1748958, AST-2106552, and NASA LPS  
<sup>15</sup> 80NSSC24K0440. S.B. is supported by the UKRI Future  
<sup>16</sup> Leaders Fellowship [grant numbers MR/V023381/1 and  
<sup>17</sup> UKRI2044] E.R. is supported by NKFIH-OTKA  
<sup>18</sup> grant K-142534 from the National Research, Development  
<sup>19</sup> and Innovation Office (NKFIH), Hungary.

## APPENDIX

Presented here are the names, symbols, and descriptions of the CAMELS 1P simulation set parameters explored in this work.

## REFERENCES

Agazie, G., et al. 2023, *Astrophys. J. Lett.*, 951, L8, doi: [10.3847/2041-8213/acdac6](https://doi.org/10.3847/2041-8213/acdac6)

Anglés-Alcázar, D., Davé, R., Faucher-Giguère, C.-A., Özel, F., & Hopkins, P. F. 2017a, *MNRAS*, 464, 2840, doi: [10.1093/mnras/stw2565](https://doi.org/10.1093/mnras/stw2565)

Anglés-Alcázar, D., Faucher-Giguère, C.-A., Kereš, D., et al. 2017b, *MNRAS*, 470, 4698, doi: [10.1093/mnras/stx1517](https://doi.org/10.1093/mnras/stx1517)

Anglés-Alcázar, D., Faucher-Giguère, C.-A., Quataert, E., et al. 2017, *Monthly Notices of the Royal Astronomical Society*, 472, L109–L114, doi: [10.1093/mnrasl/slx161](https://doi.org/10.1093/mnrasl/slx161)

Antoniadis, J., et al. 2023, *Astron. Astrophys.*, 678, A50, doi: [10.1051/0004-6361/202346844](https://doi.org/10.1051/0004-6361/202346844)

Barausse, E., Dvorkin, I., Tremmel, M., Volonteri, M., & Bonetti, M. 2020, *ApJ*, 904, 16, doi: [10.3847/1538-4357/abba7f](https://doi.org/10.3847/1538-4357/abba7f)

Bondi, H. 1952, *MNRAS*, 112, 195, doi: [10.1093/mnras/112.2.195](https://doi.org/10.1093/mnras/112.2.195)

Casey-Clyde, J. A., Mingarelli, C. M. F., Greene, J. E., et al. 2025, *ApJ*, 987, 106, doi: [10.3847/1538-4357/adce05](https://doi.org/10.3847/1538-4357/adce05)

—. 2022, *ApJ*, 924, 93, doi: [10.3847/1538-4357/ac32de](https://doi.org/10.3847/1538-4357/ac32de)

Chen, N., Di Matteo, T., Zhou, Y., et al. 2025, *ApJL*, 991, L19, doi: [10.3847/2041-8213/adefe2](https://doi.org/10.3847/2041-8213/adefe2)

Christiansen, J. F., Davé, R., Sorini, D., & Anglés-Alcázar, D. 2020, *MNRAS*, 499, 2617, doi: [10.1093/mnras/staa3007](https://doi.org/10.1093/mnras/staa3007)

Davé, R., Anglés-Alcázar, D., Narayanan, D., et al. 2019, *MNRAS*, 486, 2827, doi: [10.1093/mnras/stz937](https://doi.org/10.1093/mnras/stz937)

Di Matteo, T., Springel, V., & Hernquist, L. 2005, *Nature*, 433, 604, doi: [10.1038/nature03335](https://doi.org/10.1038/nature03335)

Dubois, Y., Volonteri, M., & Silk, J. 2015, *Monthly Notices of the Royal Astronomical Society*, 452, 1502–1518, doi: [10.1093/mnras/stv1416](https://doi.org/10.1093/mnras/stv1416)

Fabian, A. C. 2012, *ARA&A*, 50, 455, doi: [10.1146/annurev-astro-081811-125521](https://doi.org/10.1146/annurev-astro-081811-125521)

Faucher-Giguère, C.-A., Lidz, A., Zaldarriaga, M., & Hernquist, L. 2009, *ApJ*, 703, 1416, doi: [10.1088/0004-637X/703/2/1416](https://doi.org/10.1088/0004-637X/703/2/1416)

Haardt, F., & Madau, P. 2012, *ApJ*, 746, 125, doi: [10.1088/0004-637X/746/2/125](https://doi.org/10.1088/0004-637X/746/2/125)

Heckman, T. M., & Best, P. N. 2014, *ARA&A*, 52, 589, doi: [10.1146/annurev-astro-081913-035722](https://doi.org/10.1146/annurev-astro-081913-035722)

**Table 1.** Summary of the galactic feedback parameters in the CAMELS-IllustrisTNG suite. Values are sampled logarithmically unless otherwise stated. Parameters with an asterisk correspond stellar modeling while those without correspond to SMBH modeling. More details about the parameters can be found in Ni et al. (2023).

Name from Ni et al. 2023	Symbol	Description
WindEnergyIn1e51erg	$A_{SN1}^*$	Normalization factor for energy in galactic winds per unit SF. Sampled between 0.9 and 14.4 with fiducial value 3.6.
VariableWindVelFactor	$A_{SN2}^*$	Normalization factor for the galactic wind speed. Sampled between 3.7 and 14.8 with fiducial value 7.4.
RadioFeedbackFactor	$A_{AGN1}$	Normalization factor for the energy in AGN feedback per unit accretion rate in the low-accretion state. Sampled between 0.25 and 4 with fiducial value 1.
RadioFeedbackReorientationFactor	$A_{AGN2}$	Normalization factor for the frequency of AGN feedback energy release events in the low-accretion state. Sampled between 10 and 40 with fiducial value 20.
MaxSfrTimescale	$t_0^*$	Timescale for SF at the density threshold of SF. Sampled between 1.135 and 4.54 Gyr with fiducial value 2.27 Gyr
FactorForSofterEQS	$q_{EOS}^*$	Interpolation factor between the effective equation of state for SF gas. Sampled between 0.1 and 0.9 with fiducial value 0.3.
IMFslope	$\alpha^*$	Power-law index of the stellar initial mass function above $1 M_{\odot}$ . Sampled linearly between -2.8 and -1.8 with fiducial value -2.3.
SNII_MinMass_Msun	$M_{SNII,min}^*$	Lower threshold for the mass of a star that produces a SN explosion. Sampled linearly between 4 and 12 $M_{\odot}$ with fiducial value 8 $M_{\odot}$ .
ThermalWindFraction	$\tau_w^*$	Fraction of galactic wind feedback energy that is injected thermally. Sampled between 0.025 and 0.4 with fiducial value 0.1.
VariableWindSpecMomentum	$mom_w^*$	Normalization factor for the specific momentum in galactic winds per unit SF. Sampled linearly between 0 and 4000 $km\ s^{-1}$ with fiducial value 0 $km\ s^{-1}$ .
WindFreeTravelDensFac	$\rho_{w,rc}^*$	Sets the gas density around (collisionless) galactic wind particles at which they recouple back into the hydrodynamics. Sampled between 0.005 and 0.5 with fiducial value 0.05 in units of density threshold for SF.
MinWindVel	$v_{w,min}^*$	Minimum value imposed for the galactic wind speed. Sampled linearly between 150 and 550 $km\ s^{-1}$ with fiducial value of 350 $km\ s^{-1}$ .
WindEnergyReductionFactor	$f_{w,Z}^*$	Normalization factor for the energy of galactic winds at high compared to low metallicity. Sampled between 0.0625 and 1 with fiducial value 0.25.
WindEnergyReductionMetallicity	$Z_{w,ref}^*$	Sets metallicity at which transition from high- to low-energy galactic winds occurs. Sampled between 0.0005 and 0.008 with fiducial value 0.002.
WindEnergyReductionExponent	$\gamma_{w,Z}^*$	Controls abruptness in metallicity of transition between high- and low-energy galactic winds. Sampled linearly between 1 and 3 with fiducial value 2.
WindDumpFactor	$1 - \gamma_w^*$	Fraction of metals in SF cell getting ejected into a galactic wind that are deposited in neighboring SF cells prior to ejection. Sampled linearly between 0.2 and 1 with fiducial value 0.6.
SeedBlackHoleMass	$M_{BHseed}$	Mass of seed SMBHs. Sampled between $2.5 \times 10^5$ and $2.5 \times 10^6 M_{\odot}$ with fiducial value $8 \times 10^5 M_{\odot}$ .
BlackHoleAccretionFactor	$A_{Bondi}$	Normalization factor for the Bondi rate for accretion onto SMBHs. Sampled between 0.25 and 4 with fiducial value 1.
BlackHoleEddingtonFactor	$A_{Edd}$	Normalization factor for the limiting Eddington rate for accretion onto SMBHs. Sampled between 0.1 and 10 with fiducial value 1.
BlackHoleFeedbackFactor	$\epsilon_{f,high}$	Normalization factor for the energy in AGN feedback per unit accretion rate in the high-accretion state. Sampled between 0.025 and 0.4 with fiducial value 0.1.
BlackHoleRadiativeEfficiency	$\epsilon_r$	Fraction of the accretion rest-mass that is released in the accretion process. Sampled between 0.05 and 0.8 with fiducial value 0.2.
QuasarThreshold	$\chi_0$	Eddington ratio that serves as the threshold between the low- and high-accretion states of AGN feedback. Sampled between 0.000063 and 0.063 with fiducial value 0.002.
QuasarThresholdPower	$\beta$	Power-law index of scaling of the low- to high-accretion state threshold with BH mass. Sampled linearly between 0 and 4 with fiducial value 2.

**Table 2.** Summary of the galactic feedback parameters in the CAMELS-Simba suite. Values are sampled logarithmically unless otherwise stated. More details about the parameters can be found in Ni et al. (2023).

Name from Ni et al. 2023	Symbol	Description
$A_{SN1}$	-	Normalization factor for the mass loading of galactic winds. Sampled between 0.25 and 4.0 with fiducial value 1.
$A_{SN2}$	-	Normalization factor for the speed of galactic winds. Sampled between 0.5 and 2 with fiducial value 1.
$A_{AGN1}$	-	Normalization factor for the momentum flux of kinetic AGN-driven outflows. Sampled between 0.25 and 4 with fiducial value 1.
$A_{AGN2}$	-	Normalization factor for the speed of AGN-driven outflows in jet mode. Sampled between 0.5 and 2 with fiducial value 1.
SfrCritDens	$n_{\text{crit}}^*$	Gas number density threshold for SF. Sampled between 0.02 and 2 $\text{cm}^{-3}$ with fiducial value $0.2 \text{ cm}^{-3}$ .
SfrEfficiency	$\epsilon_*$	SF efficiency per free fall time. Sampled between 0.01 and 0.04 with fiducial value 0.02.
ISMJeansFac	$A_{\text{ISMngb}}$	Determines the level of artificial pressurization in the ISM. Sampled between 0.25 and 4 with fiducial value 1.
WindTravTime	$t_{rc}^*$	Maximum amount of time that galactic winds can propagate before recoupling in units of the Hubble time. Sampled between 0.2 and 0.002 with fiducial value 0.02
WindDensFac	$n_{rc}^*$	Defines gas number density threshold below which decoupled galactic winds are forced to recouple. Sampled between 0.1 and 0.001 $\text{cm}^{-3}$ with fiducial value $0.01 \text{ cm}^{-3}$ .
WindColdTemp	$T_{\text{cold}}^*$	Defines the temperature assumed for the cold phase of galactic winds. Sampled between 100 and $10^4 \text{ K}$ with fiducial value 1000 K.
WindHotFrac	$A_{\text{hot}}^*$	Fraction of wind particles ejected in the hot phase. Sampled linearly between 0 and 0.6 with fiducial value 0.3.
WindVelSlope	$\gamma_v^*$	Power-law dependence of the galactic wind velocity on the circular velocity of the galaxy. Sampled linearly between -0.38 and 0.62 with fiducial value 0.12.
AGBWindHeatVel	$v_{\text{AGB}}^*$	Velocity of winds from AGB stars which are assumed to thermalize with the ambient ISM. Sampled between 25 and 400 $\text{km s}^{-1}$ with fiducial value 100 $\text{km s}^{-1}$ .
BHSeedMass	$M_{\text{BHseed}}$	Mass of the SMBH seeds sampled between $10^3$ and $10^5 h^{-1} M_{\odot}$ with fiducial value $10^4 h^{-1} M_{\odot}$ .
BHSeedRatio	$A_{\text{BHseed}}$	Normalization factor for the minimum galaxy stellar mass required for BH seeding. Sampled between $3 \times 10^4$ and $3 \times 10^6$ with fiducial value $3 \times 10^5$ .
BHAccrFac	$A_{\text{BHaccr}}$	Normalization factor for the BH growth rate. Sampled between 0.25 and 4 with fiducial value 1.
BHAccrMaxR	$R_{\text{BHkernel}}$	Maximum size of the BH kernel used with searching for neighboring gas elements. Sampled between 2 and $8 h^{-1} \text{kpc}$ with fiducial value $4 h^{-1} \text{kpc}$ .
BHAccrTempThr	$T_{\text{AccrThr}}$	Temperature threshold above which gas accretes onto the BH at the Bondi rate. Sampled between $10^4$ and $10^6 \text{ K}$ with fiducial value $10^5 \text{ K}$ .
BHEddingtonFac	$A_{\text{torque}}$	Normalization factor for limiting Eddington rate of cold gas accretion. Sampled between 0.75 and 12 with fiducial value of 3.
BHNgFac	$A_{\text{BHngb}}$	Sets desired effective number of gas resolution elements within the BH kernel. Sampled linearly between 2 and 6 with fiducial value 4.
BHRadiativeEff	$\eta$	Radiative efficiency of the BH accretion disk. Sampled between 0.025 and 0.4 with fiducial value 0.1.
BHJetTvirVel	$v_{\text{BHvir}}$	Sets the outflow velocity above which AGN jets are heated to the virial temperature of the halo. Sampled between 500 and 8000 $\text{km s}^{-1}$ with fiducial value 2000 $\text{km s}^{-1}$ .
BHJetMassThr	$M_{\text{BHjet}}$	BH mass threshold above which BHs are allowed to transition into the jet feedback mode. Sampled between $4.5 \times 10^6$ and $4.5 \times 10^8 M_{\odot}$ with fiducial value $4.5 \times 10^7 M_{\odot}$ .

Hopkins, P. F. 2015, MNRAS, 450, 53, doi: [10.1093/mnras/stv195](https://doi.org/10.1093/mnras/stv195)

Hopkins, P. F., Kereš, D., Oñorbe, J., et al. 2014, MNRAS, 445, 581, doi: [10.1093/mnras/stu1738](https://doi.org/10.1093/mnras/stu1738)

Hopkins, P. F., & Quataert, E. 2011, MNRAS, 415, 1027, doi: [10.1111/j.1365-2966.2011.18542.x](https://doi.org/10.1111/j.1365-2966.2011.18542.x)

Katz, N., Weinberg, D. H., & Hernquist, L. 1996, The Astrophysical Journal Supplement Series, 105, 19, doi: [10.1086/192305](https://doi.org/10.1086/192305)

Kelley, L. 2024, in EAS2024, European Astronomical Society Annual Meeting, 2377

Kelley, L. Z., Blecha, L., & Hernquist, L. 2017a, MNRAS, 464, 3131, doi: [10.1093/mnras/stw2452](https://doi.org/10.1093/mnras/stw2452)

Kelley, L. Z., Blecha, L., Hernquist, L., Sesana, A., & Taylor, S. R. 2017b, MNRAS, 471, 4508, doi: [10.1093/mnras/stx1638](https://doi.org/10.1093/mnras/stx1638)

Kozhikkal, M. M., Chen, S., Theureau, G., Habouzit, M., & Sesana, A. 2024, MNRAS, 531, 1931, doi: [10.1093/mnras/stae1219](https://doi.org/10.1093/mnras/stae1219)

Kulier, A., Ostriker, J. P., Natarajan, P., Lackner, C. N., & Cen, R. 2015, ApJ, 799, 178, doi: [10.1088/0004-637X/799/2/178](https://doi.org/10.1088/0004-637X/799/2/178)

Li, Q., Narayanan, D., & Davé, R. 2019, MNRAS, 490, 1425, doi: [10.1093/mnras/stz2684](https://doi.org/10.1093/mnras/stz2684)

Marinacci, F., Baldi, M., Iorio, G., et al. 2025, arXiv e-prints, arXiv:2510.06311, doi: [10.48550/arXiv.2510.06311](https://doi.org/10.48550/arXiv.2510.06311)

McAlpine, S., Bower, R. G., Rosario, D. J., et al. 2018, MNRAS, 481, 3118, doi: [10.1093/mnras/sty2489](https://doi.org/10.1093/mnras/sty2489)

Miles, M. T., et al. 2024, Mon. Not. Roy. Astron. Soc., 536, 1489, doi: [10.1093/mnras/stae2571](https://doi.org/10.1093/mnras/stae2571)

Mingarelli, C. M. F. 2026, arXiv e-prints, arXiv:2601.18859. <https://arxiv.org/abs/2601.18859>

Muratov, A. L., Kereš, D., Faucher-Giguère, C.-A., et al. 2015, MNRAS, 454, 2691, doi: [10.1093/mnras/stv2126](https://doi.org/10.1093/mnras/stv2126)

Nelson, D., Springel, V., Pillepich, A., et al. 2019, Computational Astrophysics and Cosmology, 6, 2, doi: [10.1186/s40668-019-0028-x](https://doi.org/10.1186/s40668-019-0028-x)

Ni, Y., Chen, N., Zhou, Y., et al. 2025, ApJ, 990, 120, doi: [10.3847/1538-4357/adf3a7](https://doi.org/10.3847/1538-4357/adf3a7)

Ni, Y., Di Matteo, T., Bird, S., et al. 2022, MNRAS, 513, 670, doi: [10.1093/mnras/stac351](https://doi.org/10.1093/mnras/stac351)

Ni, Y., Genel, S., Anglés-Alcázar, D., et al. 2023, arXiv e-prints, arXiv:2304.02096, doi: [10.48550/arXiv.2304.02096](https://doi.org/10.48550/arXiv.2304.02096)

Pacucci, F., Nguyen, B., Carniani, S., Maiolino, R., & Fan, X. 2023, ApJL, 957, L3, doi: [10.3847/2041-8213/ad0158](https://doi.org/10.3847/2041-8213/ad0158)

Pakmor, R., Springel, V., Coles, J. P., et al. 2023, MNRAS, 524, 2539, doi: [10.1093/mnras/stac3620](https://doi.org/10.1093/mnras/stac3620)

Phinney, E. S. 2001, arXiv e-prints, astro, doi: [10.48550/arXiv.astro-ph/0108028](https://doi.org/10.48550/arXiv.astro-ph/0108028)

Pillepich, A., Springel, V., Nelson, D., et al. 2018, MNRAS, 473, 4077, doi: [10.1093/mnras/stx2656](https://doi.org/10.1093/mnras/stx2656)

Rahmati, A., Pawlik, A. H., Raičević, M., & Schaye, J. 2013, MNRAS, 430, 2427, doi: [10.1093/mnras/stt066](https://doi.org/10.1093/mnras/stt066)

Ravi, V., Wyithe, J. S. B., Shannon, R. M., Hobbs, G., & Manchester, R. N. 2019, Nature Astronomy, 3, 928–935, doi: [10.1038/s41550-019-0840-4](https://doi.org/10.1038/s41550-019-0840-4)

Reardon, D. J., et al. 2023, Astrophys. J. Lett., 951, L6, doi: [10.3847/2041-8213/acdd02](https://doi.org/10.3847/2041-8213/acdd02)

Rosas-Guevara, Y. M., Bower, R. G., Schaye, J., et al. 2015, MNRAS, 454, 1038, doi: [10.1093/mnras/stv2056](https://doi.org/10.1093/mnras/stv2056)

Sato-Polito, G., & Zaldarriaga, M. 2025, PhRvD, 111, 023043, doi: [10.1103/PhysRevD.111.023043](https://doi.org/10.1103/PhysRevD.111.023043)

Schaye, J., Crain, R. A., Bower, R. G., et al. 2015, MNRAS, 446, 521, doi: [10.1093/mnras/stu2058](https://doi.org/10.1093/mnras/stu2058)

Schmidt, M. 1963, Nature, 197, 1040, doi: [10.1038/1971040a0](https://doi.org/10.1038/1971040a0)

Sesana, A. 2013, Monthly Notices of the Royal Astronomical Society, 433, L1–L5, doi: [10.1093/mnrasl/slt034](https://doi.org/10.1093/mnrasl/slt034)

Sesana, A., Vecchio, A., & Colacino, C. N. 2008, Monthly Notices of the Royal Astronomical Society, 390, 192–209, doi: [10.1111/j.1365-2966.2008.13682.x](https://doi.org/10.1111/j.1365-2966.2008.13682.x)

Sijacki, D., Vogelsberger, M., Genel, S., et al. 2015, MNRAS, 452, 575, doi: [10.1093/mnras/stv1340](https://doi.org/10.1093/mnras/stv1340)

Smith, B. D., Bryan, G. L., Glover, S. C. O., et al. 2017, MNRAS, 466, 2217, doi: [10.1093/mnras/stw3291](https://doi.org/10.1093/mnras/stw3291)

Springel, V. 2010, MNRAS, 401, 791, doi: [10.1111/j.1365-2966.2009.15715.x](https://doi.org/10.1111/j.1365-2966.2009.15715.x)

Springel, V., Di Matteo, T., & Hernquist, L. 2005, MNRAS, 361, 776, doi: [10.1111/j.1365-2966.2005.09238.x](https://doi.org/10.1111/j.1365-2966.2005.09238.x)

Springel, V., & Hernquist, L. 2003, MNRAS, 339, 289, doi: [10.1046/j.1365-8711.2003.06206.x](https://doi.org/10.1046/j.1365-8711.2003.06206.x)

Steinborn, L. K., Dolag, K., Hirschmann, M., Prieto, M. A., & Remus, R.-S. 2015, MNRAS, 448, 1504, doi: [10.1093/mnras/stv072](https://doi.org/10.1093/mnras/stv072)

Sunseri, J., Andalman, Z. L., & Teyssier, R. 2025, arXiv e-prints, arXiv:2510.19822, doi: [10.48550/arXiv.2510.19822](https://doi.org/10.48550/arXiv.2510.19822)

Sykes, B., Middleton, H., Melatos, A., et al. 2022, MNRAS, 511, 5241, doi: [10.1093/mnras/stac388](https://doi.org/10.1093/mnras/stac388)

Tillman, M. T., Burkhart, B., Tonnesen, S., Bird, S., & Bryan, G. L. 2025, ApJ, 980, 72, doi: [10.3847/1538-4357/ada5f7](https://doi.org/10.3847/1538-4357/ada5f7)

Tillman, M. T., Burkhart, B., Tonnesen, S., et al. 2023, ApJL, 945, L17, doi: [10.3847/2041-8213/acb7f1](https://doi.org/10.3847/2041-8213/acb7f1)

Villaescusa-Navarro, F., Anglés-Alcázar, D., Genel, S., et al. 2021, ApJ, 915, 71, doi: [10.3847/1538-4357/abf7ba](https://doi.org/10.3847/1538-4357/abf7ba)

Villaescusa-Navarro, F., Genel, S., Anglés-Alcázar, D., et al. 2023, *ApJS*, 265, 54, doi: [10.3847/1538-4365/acbf47](https://doi.org/10.3847/1538-4365/acbf47)

Vogelsberger, M., Genel, S., Sijacki, D., et al. 2013, *MNRAS*, 436, 3031, doi: [10.1093/mnras/stt1789](https://doi.org/10.1093/mnras/stt1789)

Vogelsberger, M., Sijacki, D., Kereš, D., Springel, V., & Hernquist, L. 2012, *MNRAS*, 425, 3024, doi: [10.1111/j.1365-2966.2012.21590.x](https://doi.org/10.1111/j.1365-2966.2012.21590.x)

Weinberger, R., Springel, V., & Pakmor, R. 2020, *ApJS*, 248, 32, doi: [10.3847/1538-4365/ab908c](https://doi.org/10.3847/1538-4365/ab908c)

Weinberger, R., Springel, V., Pakmor, R., et al. 2018, *MNRAS*, 479, 4056, doi: [10.1093/mnras/sty1733](https://doi.org/10.1093/mnras/sty1733)

Weinberger, R., Su, K.-Y., Ehlert, K., et al. 2023, *MNRAS*, 523, 1104, doi: [10.1093/mnras/stad1396](https://doi.org/10.1093/mnras/stad1396)

White, S. D. M., & Rees, M. J. 1978, *MNRAS*, 183, 341, doi: [10.1093/mnras/183.3.341](https://doi.org/10.1093/mnras/183.3.341)

Xu, H., et al. 2023, *Res. Astron. Astrophys.*, 23, 075024, doi: [10.1088/1674-4527/acdfa5](https://doi.org/10.1088/1674-4527/acdfa5)